



Universiteit
Leiden
The Netherlands

Anisotropy in cell mechanics

Schakenraad, K.K.

Citation

Schakenraad, K. K. (2020, May 13). *Anisotropy in cell mechanics. Casimir PhD Series*. Retrieved from <https://hdl.handle.net/1887/87895>

Version: Publisher's Version

License: [Licence agreement concerning inclusion of doctoral thesis in the Institutional Repository of the University of Leiden](#)

Downloaded from: <https://hdl.handle.net/1887/87895>

Note: To cite this publication please use the final published version (if applicable).

Cover Page



Universiteit Leiden



The handle <http://hdl.handle.net/1887/87895> holds various files of this Leiden University dissertation.

Author: Schakenraad, K.K.

Title: Anisotropy in cell mechanics

Issue Date: 2020-05-13

Part I

Mechanics of the cytoskeleton

CYTOSKELETAL ANISOTROPY CONTROLS GEOMETRY AND FORCES OF ADHERENT CELLS

This chapter is the result of a collaboration with Wim Pomp, Hayri E. Balcioglu, Hedde van Hoorn, Erik H.J. Danen, and Thomas Schmidt, who performed the experiments and analyzed the experimental data. The chapter is reprinted with permission, copyright 2018 by the American Physical Society. The chapter is published as:

Wim Pomp*, Koen Schakenraad*, Hayri E. Balcioglu, Hedde van Hoorn, Erik H.J. Danen, Roeland M.H. Merks, Thomas Schmidt, and Luca Giomi, 'Cytoskeletal Anisotropy Controls Geometry and Forces of Adherent Cells', *Physical Review Letters* **121**, 178101 (2018)

Abstract

We investigate the geometrical and mechanical properties of adherent cells characterized by a highly anisotropic actin cytoskeleton. Using a combination of theoretical work and experiments on micropillar arrays, we demonstrate that the shape of the cell edge is accurately described by elliptical arcs, whose eccentricity expresses the degree of anisotropy of the internal cell stresses. This results in a spatially varying tension along the cell edge, that significantly affects the traction forces exerted by the cell on the substrate. Our work highlights the strong interplay between cell mechanics and geometry and paves the way toward the reconstruction of cellular forces from geometrical data.

*These authors contributed equally to this work

2.1 Introduction

Cells, from simple prokaryotes to the more complex eukaryotes, are capable of astonishing mechanical functionalities. They can repair wounded tissues by locally contracting the extracellular matrix [159], move in a fluid or on a substrate [160], and generate enough force to split themselves in two while remaining alive [161]. Conversely, cell behavior and fate crucially depend on mechanical cues from outside the cell [162–166]. Examples include rigidity-dependent stem cell differentiation [28, 30], protein expression regulated by internal stresses [167], mechanical cell-cell communication [168] and durotaxis [132, 169]. In all these biomechanical processes, cells rely on their shape [64, 170, 171] to gauge the mechanical properties of their microenvironment [172] and direct the traction forces exerted on their surroundings.

In recent years, experiments on adhesive surfaces have contributed to explore such mechanical complexity in a controlled setting [48]. Immediately after coming into contact with such a surface, many animal cells spread and develop transmembrane adhesion receptors. This induces the actin cytoskeleton to reorganize into cross-linked networks and bundles (i.e., stress fibers [46, 47]), whereas adhesion becomes limited to a number of sites, distributed mainly along the cell contour (i.e., focal adhesions [54]). At this stage, cells are essentially flat and assume a typical shape characterized by arcs which span between the sites of adhesion, while forces are mainly contractile [48]. On timescales much shorter than those required by a cell to change its shape (i.e., minutes), the cell can be considered in mechanical equilibrium at any point of its interface. These observations have opened the way to the use of theoretical concepts inspired by the physics of fluid interfaces [48, 62–64], but limited to the case of cells with an isotropic cytoskeleton.

In this chapter, we overcome this limitation and explore the geometry and the mechanical properties of adherent cells characterized by a highly anisotropic actin cytoskeleton. Using a combination of theoretical modeling, spinning disk confocal microscopy, and traction-force microscopy of living cells cultured on microfabricated elastomeric pillar arrays [55–57], we demonstrate that both the shape of and the traction forces exerted by adherent cells are determined by the anisotropy of their actin cytoskeleton. In particular, by comparing different cell types [173], we demonstrate that the cell contour consists of arcs of a unique ellipse, whose eccentricity expresses the degree of anisotropy of the internal stresses.

2.2 The model

We model adherent cells as two-dimensional contractile films [65, 66], and we focus on the shape of the cell edge connecting two consecutive adhesion sites. Mechanical equilibrium requires the difference between the internal and external stresses acting on the cell edge to balance the contractile forces arising in the cortex:

$$\frac{d\mathbf{F}_{\text{cortex}}}{ds} + (\hat{\Sigma}_{\text{out}} - \hat{\Sigma}_{\text{in}}) \cdot \mathbf{N} = \mathbf{0} . \quad (2.1)$$

Here $\hat{\Sigma}_{\text{out}}$ and $\hat{\Sigma}_{\text{in}}$ are the stress tensors outside and inside the cell and $\mathbf{F}_{\text{cortex}}$ is the stress resultant along the cell cortex. The latter is parametrized as a one-dimensional curve spanned by the arc-length s and oriented along the inward pointing normal vector \mathbf{N} . A successful approach, initially proposed by Bar-Ziv *et al.* in the context of cell pearling [62] and later expanded by Bischofs *et al.* [63, 64], consists of modeling bulk contractility in terms of an isotropic pressure $\hat{\Sigma}_{\text{out}} - \hat{\Sigma}_{\text{in}} = \sigma \hat{\mathbf{I}}$, with $\hat{\mathbf{I}}$ the identity matrix, and peripheral contractility as an interfacial tension of the form $\mathbf{F}_{\text{cortex}} = \lambda \mathbf{T}$, with \mathbf{T} a unit vector tangent to the cell edge. The quantities σ and λ are material constants that embody the biomechanical activity of myosin motors in the actin cytoskeleton. This competition between bulk and peripheral contractility along the cell boundary results in the formation of arcs of constant curvature $1/R = \sigma/\lambda$, through a mechanism analogous to the Young-Laplace law for fluid interfaces. The shape of the cell boundary is then approximated by a sequence of circular arcs, whose radius R might or might not be uniform across the cell, depending on how the cortical tension λ varies from arc to arc. The possibility of an elastic origin of the cortical tension was also explored in Ref. [63] to account for an apparent correlation between the curvature and length L of the cellular arcs. In this case $\lambda = k(L - L_0)/L_0$, with k an elastic constant and L_0 a rest length. Both models successfully describe the geometry of adherent cells in the presence of strictly isotropic forces.

Yet, many cells, including the fibroblastoids (GD β 1, GD β 3) and epithelioids (GE β 1, GE β 3) [173] studied here [Figure 2.1a], develop directed forces by virtue of the strong anisotropic cytoskeleton originating from the actin stress fibers [46, 47]. This scenario is, evidently, beyond the scope of models based on isotropic contractility. Indeed, long cellular arcs appear prominently non-circular, as indicated by the fact that their curvature smoothly varies along the arc up to a factor ten [Figure 2.5a in the Appendix]. Furthermore, whereas the shape of the cell edge in Figure 2.1a can in principle be approximated by circular arcs, a survey of a sample of 285 cells [Figure 2.5b in the Appendix] did not allow conclusive statements about a possible correlation between the arc's length and curvature, required to justify the variance in λ [63, 64]. On the other hand, our data show a significant correlation between the radius of curvature of the cellular arcs and their orientation with respect to the stress fibers [Figure 2.1b]. In particular, the radius of curvature decreases as the stress fibers become more perpendicular to the cell cortex [Figure 2.1c]. This correlation is intuitive as the bulk contractile stress focuses in the direction of the stress fibers.

The anisotropy of the actin cytoskeleton can be incorporated into the mechanical framework summarized by Eq. (2.1), by modeling the stress fibers as contractile force dipoles. This collectively gives rise to a directed contractile bulk stress, such that $\hat{\Sigma}_{\text{out}} - \hat{\Sigma}_{\text{in}} = \sigma \hat{\mathbf{I}} + \alpha \mathbf{n}\mathbf{n}$ [102, 103, 174], with $\mathbf{n} = (\cos \theta_{\text{SF}}, \sin \theta_{\text{SF}})$ the average direction of the stress fibers [Figure 2.1b]. The quantity $\alpha > 0$ represents the magnitude of the directed contractile stresses and is proportional to the local degree of alignment between the fibers. The higher the alignment, the larger α , whereas in the case of randomly oriented fibers $\alpha = 0$, thus recovering the isotropic case. The ratio between isotropic contractility

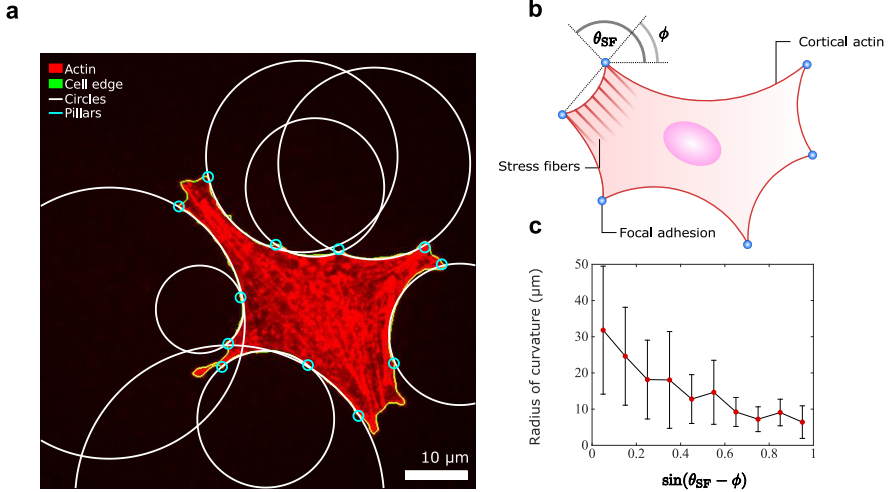


Figure 2.1. (a) A cell with an anisotropic actin cytoskeleton (epithelioid GEβ3) with circles (white) fitted to its edges (green). The end points of the arcs (cyan) are identified based on the forces exerted on the pillars, see Materials and Methods in Section 2.5. The actin cytoskeleton is visualized with tetramethyl isothiocyanate rhodamine phalloidin (red). Scale bar is 10 μm . (b) The cell cortex (red line) is spanned in segments between fixed adhesion sites (blue). (c) Arc radius as a function of the sine of the angle $\theta_{\text{SF}} - \phi$, between the local orientation of the stress fibers and that of the distance between the adhesion sites (data correspond to a sample of 285 cells and show the mean \pm standard deviation).

σ and directed contractility α measures the degree of anisotropy of the bulk stress. With this stress tensor the force balance [Eq. (2.1)] becomes

$$\frac{d\lambda}{ds} \mathbf{T} + (\lambda\kappa + \sigma)\mathbf{N} + \alpha(\mathbf{n} \cdot \mathbf{N})\mathbf{n} = \mathbf{0}, \quad (2.2)$$

where we use $d\mathbf{T}/ds = \kappa\mathbf{N}$, with κ the curvature of the cell edge. This implies that, in the presence of an anisotropic cytoskeleton, the cortical tension λ is no longer constant along the cell cortex, as long as the directed stress has a non-vanishing tangential component (i.e., $\mathbf{n} \cdot \mathbf{T} \neq 0$). As shown by Kassianidou *et al.* [175], isolated stress fibers can also exert localized contractile forces on the cell contour, leading to kinks and piecewise constant curvature. Consistent with our experiments, here we consider the case in which the density of the stress fibers is sufficiently high and uniform to approximate their mechanical effect in terms of a continuous anisotropic stress.

2.3 Results and discussion

In the following, we introduce a number of simplifications that make the problem analytically tractable. As the orientation of the stress fibers varies only slightly along a single cellular arc [Figure 2.2a, and Figures 2.7 and 2.8 in the Appendix], we assume θ_{SF} to be constant along each arc, but different, in general, from arc to arc. Furthermore, as all the arcs share the same bulk, we assume the bulk stresses σ and α uniform throughout the cell. Under these assumptions a general solution of Eq. (2.2) can be readily obtained. Taking $\mathbf{T} = (\cos \varphi, \sin \varphi)$, $\mathbf{N} = (-\sin \varphi, \cos \varphi)$, with φ the orientation of the tangent vector \mathbf{T} with respect to an axis perpendicular to the stress fibers [Figure 2.2a], and $\tan \varphi = dy/dx$, with (x, y) the position of the cell contour, yields:

$$\frac{\sigma^2}{\gamma \lambda_{\min}^2} [(x - x_c) \sin \theta_{\text{SF}} - (y - y_c) \cos \theta_{\text{SF}}]^2 + \frac{\sigma^2}{\lambda_{\min}^2} [(x - x_c) \cos \theta_{\text{SF}} + (y - y_c) \sin \theta_{\text{SF}}]^2 = 1, \quad (2.3)$$

where $\gamma = \sigma/(\sigma + \alpha)$ and λ_{\min} is an integration constant related with cortical tension and whose physical interpretation will become clear later. Eq. (2.3) describes an ellipse of semiaxes $a = \sqrt{\gamma} \lambda_{\min}/\sigma$ and $b = \lambda_{\min}/\sigma$, centered at the point (x_c, y_c) and whose major axis is parallel to the stress fibers, hence tilted by an angle θ_{SF} with respect to the x axis (Figure 2.2). The dimensionless quantity γ highlights the anisotropy of the forces acting on the cell contour. Thus, $\gamma = 0$ corresponds to the case in which the directed forces outweigh the isotropic ones, whereas $\gamma = 1$ reflects the purely isotropic case. Further details can be found in Section 2.6.1 in the Appendix and in Chapter 3.

The key prediction of our model is illustrated in Figure 2.2b, where we have fitted the contour of the same cell shown in Figure 2.1a with ellipses. More examples are shown in Figures 2.7 and 2.8 in the Appendix. Whereas large variations in the circles' radii were required in Figure 2.1a, a *unique* ellipse ($\gamma = 0.52$, $\lambda_{\min}/\sigma = 13.4 \mu\text{m}$) faithfully describes all the arcs in the cell. The directions of the major axes were fixed to be parallel to the local orientations of the stress fibers in the fit. To test the accuracy of this latter choice, we fitted unconstrained and independent ellipses to all cellular arcs in our database. The distribution of the difference between the orientation θ_{ellipse} of the major axis of the fitted ellipse and the measured orientation θ_{SF} of the stress fibers is shown in Figure 2.2c. The distribution peaks at 0° and has a width of 36° , demonstrating that the orientation of the ellipses is parallel, on average, to the local orientation of the stress fibers as predicted by our model.

Eq. (2.2) further allows to analytically calculate the cortical tension λ . Namely,

$$\lambda(\varphi) = \lambda_{\min} \sqrt{\frac{1 + \tan^2 \varphi}{1 + \gamma \tan^2 \varphi}}. \quad (2.4)$$

The function λ attains its minimum value at the point along the cellular arc where $\varphi = 0$ and $\lambda(0) = \lambda_{\min}$, see also Figure 2.6 in the Appendix. Here, the cortical tension has no

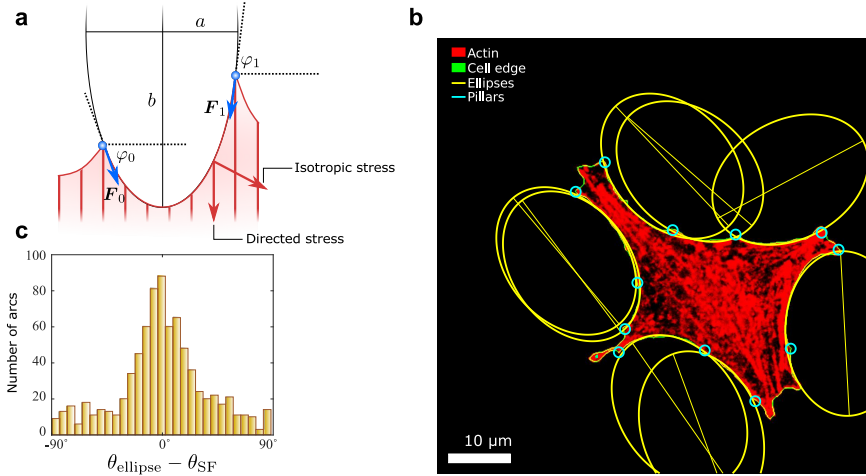


Figure 2.2. (a) Schematic representation of our model for $\theta_{SF} = \pi/2$. All cellular arcs are part of a unique ellipse of aspect ratio $a/b = \sqrt{\gamma}$. The cell exerts forces F_0 and F_1 on the adhesion sites (blue) with magnitude $\lambda(\varphi_0)$ and $\lambda(\varphi_1)$. (b) An epithelioid cell (GEβ3; same cell as in Figure 2.1a) with a unique ellipse (yellow) fitted to its edges (green). The end points of the arcs (cyan) are identified based on the forces exerted on the pillars, see Materials and Methods in Section 2.5. The fitted values of the ellipses' major and minor axes are, respectively, $13.38 \pm 0.04 \mu\text{m}$ and $9.65 \pm 0.02 \mu\text{m}$. The major axes (yellow lines) are parallel to the stress fibers. Their orientations are found to be, in counterclockwise order from the nearly vertical ellipse in the bottom right corner, $\theta_{SF} = 93 \pm 4^\circ, 28 \pm 5^\circ, 110 \pm 2^\circ, 139 \pm 6^\circ, 127 \pm 3^\circ, 125 \pm 2^\circ, 133 \pm 2^\circ, 130 \pm 3^\circ$ with respect to the horizontal axis of the image. Scalebar is $10 \mu\text{m}$. (c) Histogram of $\theta_{\text{ellipse}} - \theta_{SF}$, with θ_{ellipse} the orientation of the major axis of the fitted ellipse and θ_{SF} the measured orientation of the stress fibers. The mean of this distribution is 0° and the standard deviation is 36° .

contribution from the directed stress (i.e., $\mathbf{n} \cdot \mathbf{T} = 0$), thus λ_{\min} represents the minimal tension withstood by the cortical actin. Although the latter could, in principle, be arc-dependent, for instance in the presence of substantial variations in the actin densities [63], here we approximate λ_{\min} as a constant. Thus σ , α and λ_{\min} represent the material parameters of our model.

Eqs. (2.3) and (2.4) are combined to predict the traction force exerted by the cell at a specific adhesion site by adding the cortical tension λT along the two cellular arcs joining at the adhesion site. We emphasize that this analysis yields information on cellular forces solely based on the analysis of cell shape. For example, the direction of the traction forces is calculated without additional fitting parameters. We compare the result with the direction of the traction force measured with a micropillar array technology [55–57]. An example is shown in Figure 2.3a for one of the adhesion sites of the cell in Figure 2.2b; more examples are shown in Figures 2.7 and 2.8 in the Appendix. The

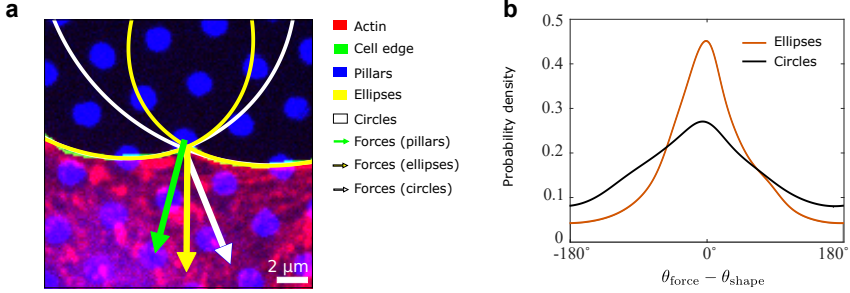


Figure 2.3. (a) Enlargement of one adhesion site of the cell in the previous figures. Actin is shown in red, the cell edge in green, and the tops of the micropillars in blue. The lines represent the fitted circle (white) and ellipse (yellow). The arrows correspond to the measured forces (green) and the predicted directions (but not magnitudes) of the forces in the presence of isotropic ($\alpha = 0$, white arrow) and anisotropic ($\alpha \neq 0$, yellow arrow) contractile stresses. Scale bar is $2 \mu\text{m}$. (b) Histogram (shown as a probability density) of $\theta_{\text{force}} - \theta_{\text{shape}}$ for isotropic (black) and anisotropic (orange) contractile stresses. Both the distributions are centered around 0° , the standard deviations are 60° and 40° for the isotropic and anisotropic models, respectively.

arrows mark the direction of the measured traction force (green) and that calculated by approximating the cell shape with ellipses (yellow). As a comparison, Figure 2.3a also shows a prediction based on circles from the isotropic model (white) [63, 64].

In Figure 2.3b, we show the distribution of the difference $\theta_{\text{force}} - \theta_{\text{shape}}$ between the measured orientation of the traction forces and that calculated from our model, across the entire cell population. The predicted distribution is centered at 0° and has a width of 40° . As a comparison, we also plot the result for the isotropic model, which displays a larger standard deviation of about 60° . This shows that not only cell shape, but also adhesion forces are profoundly affected by the anisotropy of the cytoskeleton.

Finally, our model allows us to obtain quantitative information on the relative magnitude of isotropic and anisotropic stresses. In Tables 2.1 and 2.2 (Appendix) we report a survey of the material parameters over a sample of 285 cells. Despite the large variability among the cell population, the directed stress α is consistently larger than the isotropic stress σ , reflecting the high anisotropy of the adherent cell types used here.

Table 2.1. Survey of the average material parameters in a sample of 285 fibroblastoid and epithelioid cells.

γ	λ_{min} (nN)	σ (nN/ μm)	α (nN/ μm)
0.33 ± 0.20	7.6 ± 5.6	0.87 ± 0.70	1.7 ± 1.7

2.4 Conclusion

In conclusion, we have investigated the geometrical and mechanical properties of adherent cells characterized by an anisotropic actin cytoskeleton, by combining experiments on micropillar arrays with simple mechanical modeling. We have predicted and tested that the shape of the cell edge consists of arcs that are described by a unique ellipse, whose major axis is parallel to the orientation of the stress fibers. The model allowed us to obtain quantitative information on the values of the isotropic and anisotropic contractility of cells. In the future, we plan to use our model in combination with experiments on micropatterns (see, e.g., Refs. [58, 176]), where cellular shape can be controlled, thus allowing higher reproducibility of the results and more systematic statistical analysis of the data.

2.5 Materials and methods

2.5.1 Cell culture and fluorescent labeling

Epithelioid GE11 and fibroblastoid GD25 cells [173] expressing either $\alpha 5\beta 1$ or $\alpha v\beta 3$ (GD $\beta 1$, GD $\beta 3$, GE $\beta 1$ and GE $\beta 3$) have been cultured as described before [172]. GD $\beta 1$, GD $\beta 3$, GE $\beta 1$ and GE $\beta 3$ are approximately equally represented among the 285 cells in the data presented here. Cells have cultured in medium (DMEM; Dulbecco's Modified Eagle's Medium, Invitrogen/Fisher Scientific) supplemented with 10% fetal bovine serum (HyClone, Etten-Leur, The Netherlands), 25 U/ml penicillin and 25 $\mu\text{g}/\text{ml}$ streptomycin (Invitrogen/Fisher Scientific cat. # 15070-063). Cells were fixed in 4% formaldehyde and then permeabilised with 0.1% Triton-X and 0.5% BSA in PBS. Tetramethylrhodamine (TRITC)-Phalloidin (Fisher Emergo B.V. cat. # A12380, Thermo Fisher) was subsequently used to stain F-actin.

2.5.2 Micropillar arrays

Micropillar arrays were made out of a soft elastomeric material (PDMS) using a negative silicon wafer as a mask as described before [55, 57]. Briefly, the 2 μm diameter micropillars are arranged in a hexagonal pattern with a 4 μm center-to-center distance. The micropillars have a height of 6.9 μm , resulting in a stiffness of 16.2 nN/ μm . The pillar tops were fluorescently labelled using an Alexa 405-fibronectin conjugate (Alexa Fluor®, Invitrogen/Fisher Scientific, Breda, The Netherlands; Fibronectin cat. #1141, Sigma Aldrich, Zwijndrecht, The Netherlands). Pillar deflections were determined with ~ 30 nm precision using a specifically designed Matlab script resulting in a ~ 0.5 nN precision in force [55].

2.5.3 Imaging

High-resolution imaging was performed on an in-house constructed spinning disk confocal microscope based on an Axiovert200 microscope body with a Zeiss Plan-Apochromat $100\times$ 1.4NA objective (Zeiss, Sliedrecht, The Netherlands) and a CSU-X1 spinning disk unit (CSU-X1, Yokogawa, Amersfoort, The Netherlands). Imaging was done using an emCCD camera (iXon 897, Andor, Belfast, UK). Alexa405 and TRITC were excited using 405 nm (Crystalaser, Reno, NV) and 561 nm (Cobolt, Stockholm, Sweden) lasers, respectively. This results in a resolution of approximately 150 nm and 200 nm respectively, enough to distinguish separate stress fibers which are typically separated by about 1.5 μm .

2.5.4 Image analysis

All image analysis and ellipse fitting are performed using Matlab[®], except the determination of the stress fiber orientation, for which ImageJ with the OrientationJ plugin [177] was used. The micropillar array allows measuring forces that the cell exerts on the substrate. We selected the pillars used for the force calculations and the geometrical fit shown in Figures 2.7 and 2.8 according to the following criteria. 1) They are within 10 pixels (1.38 μm) from the edge of the cell. 2) They are subject to a force that is at least 3 times larger than the average force on all the pillars or the tangent vector along the cell contour rotates by an angle equal or larger than 30° at the location of that pillar. 3) The distance between two pillars delimiting the same ellipse is larger than 50 pixels (6.9 μm). Figure 2.9 shows examples of the pillars identified with these criteria for the six cells displayed in Figures 2.7 and 2.8.

2.5.5 Ellipse fitting

Ellipses are fitted, using Matlab, to the part of the cell edge delimited by two consecutive pillars, provided the pillars satisfy the three criteria listed in Section 2.5.4. Each ellipse is described by five parameters: the two coordinates of the center, the two semi-axes and the orientation of the ellipse's longitudinal direction. In fitting ellipses to cellular arcs, the orientation of the longitudinal direction of a given ellipse is constrained to be equal to the local orientation of stress fibers along that cellular arc, consistent with our predictions [Eq. (2.3)]. This local stress fiber orientation is measured from the channel with TRITC-Phalloidin (Actin) using the OrientationJ plugin for ImageJ [177]. The average orientation per cell edge segment is calculated over all pixels between 15 and 50 pixels (2.07 μm and 6.9 μm) away from the corresponding cell edge and whose coherency is larger than 0.15. See also Section 2.5.7. Then, each cellular arc is fitted separately to obtain the coordinates of the center and the lengths of the two semi-axes of the ellipse, and the resulting lengths are averaged over the N ellipses in the cell that meet the criteria listed above. The resulting numbers serve as initial parameters for a global fit, which simultaneously fits N cellular arcs to a unique ellipse. This global fit then finds

optimal values for the coordinates of the center of each ellipse, and for the length of the two semi-axes of the unique ellipse, by minimizing the distance between fitted ellipses and the cellular arcs using χ^2 . All reported ellipse parameters are obtained using this global fit. Ellipses whose χ^2 is greater than 10 were discarded, which occurs in case of membrane ruffling and other out-of-equilibrium events.

2.5.6 Force analysis

For both isotropic and anisotropic cells, traction forces can be calculated by summing the cortical tension $\mathbf{F} = \lambda \mathbf{T}$ of the two arcs meeting at a specific adhesion site. In the anisotropic case, this is conveniently done by first rotating the ellipse in such a way the minor and major axes are parallel to the x - and y -direction respectively. Then two forces \mathbf{F}_1 and \mathbf{F}_0 are calculated by combining Eqs. (2.3) and (2.4) and defined in such a way that they are pointing clockwise and counter-clockwise around the ellipse:

$$\frac{\mathbf{F}_0}{\lambda_{\min}} = \left(\frac{d}{2b} \sin \phi + \frac{\rho}{b} \cos \phi \right) \hat{\mathbf{x}} + \left(-\frac{1}{\gamma} \frac{d}{2b} \cos \phi + \frac{\rho}{b} \sin \phi \right) \hat{\mathbf{y}}, \quad (2.5a)$$

$$\frac{\mathbf{F}_1}{\lambda_{\min}} = \left(\frac{d}{2b} \sin \phi - \frac{\rho}{b} \cos \phi \right) \hat{\mathbf{x}} + \left(-\frac{1}{\gamma} \frac{d}{2b} \cos \phi - \frac{\rho}{b} \sin \phi \right) \hat{\mathbf{y}}, \quad (2.5b)$$

where d is the distance between the positions of both forces on the ellipse, b is the major semi-axis of the ellipse and ϕ is the angle that the line through both points makes with the x -axis (see Figure 2.4). The length scale ρ is defined as:

$$\rho = \sqrt{b^2 \left(\frac{1 + \tan^2 \phi}{1 + \gamma \tan^2 \phi} \right) - \frac{1}{\gamma} \left(\frac{d}{2} \right)^2}. \quad (2.6)$$

Then, \mathbf{F}_0 and \mathbf{F}_1 are rotated back to the coordinate system of the image and summed to give the force, scaled by λ_{\min} , acting on the cell edge on the location of a particular intersection of two ellipses.

The magnitude of the traction forces is required for the calculation of the minimal line tension λ_{\min} and the isotropic and directed stresses σ and α . We get this from the micropillar array. A measured force usually is the sum of two forces exerted by two different cell edge segments. Therefore, we first decompose the traction force into two forces pointing along tangents to the two cell edge segments adjacent to the position of the force. Then, per cell, we take any combination of two clockwise and counter-clockwise forces and calculate:

$$\lambda_{\min} = \sqrt{\frac{F_{1x}^2 F_{0y}^2 - F_{0x}^2 F_{1y}^2}{F_{0y}^2 - F_{1y}^2}}, \quad \sigma = \frac{|\mathbf{F}_0 - \mathbf{F}_1|}{d} \frac{F_{0x} + F_{1x}}{F_{0y} - F_{1y}}, \quad \alpha = \sigma \left(\frac{1}{\gamma} - 1 \right). \quad (2.7)$$

Here \mathbf{F}_0 and \mathbf{F}_1 are defined in the coordinate system where the x - and y -axes are the minor and major axes of the ellipse. Furthermore, F_{nx} and F_{ny} are the components of

F_n in the x and y-directions respectively. To calculate values for these quantities, we average all the different tensions and stresses we get for all possible combinations in all cells, taking the errors on these values into account as weights while averaging.

2.5.7 Orientational analysis of the stress fibers

The local orientation of the stress fibers and their degree of alignment (see, also, Figure 2.10 in the Appendix) have been calculated using the ImageJ plugin OrientationJ [177]. The local alignment has been calculated through the following procedure. Let $I(x_0, y_0)$ be the intensity of the image at the point (x_0, y_0) and $I_u = \mathbf{u} \cdot \nabla I$, the projection on the gradient of I along the arbitrary \mathbf{u} direction. The amount of anisotropy of the image can be quantified by introducing the extrema of the squared norm of I_u , namely:

$$\Lambda_{\max} = \max_{\mathbf{u}} \|I_u\|^2, \quad \Lambda_{\min} = \min_{\mathbf{u}} \|I_u\|^2, \quad (2.8)$$

where $\|\cdot\| = \int w(x, y) dx dy (\cdot\cdot\cdot)$ represents the norm of a weighted average with $w(x, y)$ a Gaussian with a standard deviation of five pixels ($0.69 \mu\text{m}$) centered at (x_0, y_0) . The amount of anisotropy is then naturally quantified in terms of the coherence parameter:

$$C = \frac{\Lambda_{\max} - \Lambda_{\min}}{\Lambda_{\max} + \Lambda_{\min}}. \quad (2.9)$$

In case of isotropic distributions, $\Lambda_{\max} = \Lambda_{\min}$ and $C = 0$. On the other hand, in case of strongly aligned stress fibers $\Lambda_{\max} \gg \Lambda_{\min}$ and $C \approx 1$. From the right column of Figure 2.10, we see that the stress fibers are highly aligned in the periphery of the cell, consistent with our theoretical model.

2.6 Appendix

2.6.1 Angular coordinates of the adhesion sites

As we explained in Section 2.3, the ratios $b = \lambda_{\min}/\sigma$ between the peripheral and bulk contractility and $\gamma = \sigma/(\sigma + \alpha)$ between isotropic and directed stresses set, respectively, the major semi-axis and the aspect ratio $a/b = \sqrt{\gamma}$ of the ellipse approximating the shape of the cellular arcs, whereas the orientation of the ellipse is determined by the direction of the stress fibers. These quantities uniquely identify the shape and the orientation of the ellipse, but not which portion of the ellipse corresponds to a given cellular arc. In order for this to be uniquely determined, one needs to specify the relative position $\mathbf{d} = d(\cos \phi, \sin \phi)$ of the adhesion sites (Figure 2.4a), where the stress fibers are assumed, without loss of generality, parallel to the y -axis.

Then, using Eq. (2.3) with $\theta_{\text{SF}} = \pi/2$, one can straightforwardly calculate the coordinates of the center of the ellipse in the reference frame centered at the first adhesion

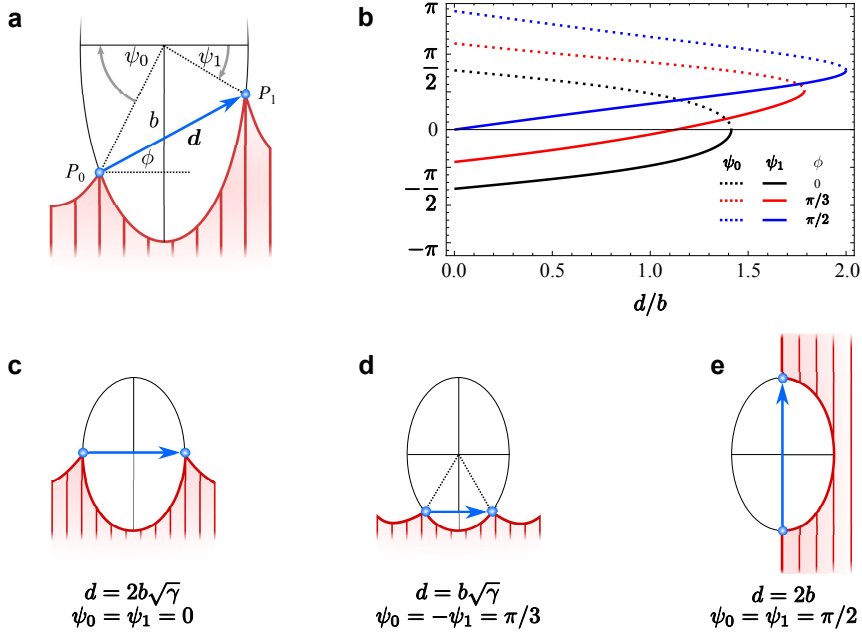


Figure 2.4. Angular coordinates of the adhesion sites. (a) Schematic illustration of a cellular arc and the approximating ellipse. The angular coordinates ψ_0 and ψ_1 are measured with respect to the negative and positive x -direction respectively. Thus, in the displayed configuration $\psi_0 > 0$ and $\psi_1 < 0$. The ellipse major semi-axis is set by the ratio between peripheral and bulk contractile stresses, i.e., $b = \lambda_{\min}/\sigma$. (b) Angular coordinates ψ_0 (dotted line) and ψ_1 (solid line) as a function of the rescaled distance between the adhesion sites, i.e., d/b , for various choices of the tilt angle ϕ and $\sigma = \alpha$ (hence $\gamma = 1/2$). (c), (d) and (e) Examples of specific configurations for various choices of d and ϕ .

site (P_0 in Figure 2.4a), namely:

$$x_c = \frac{d}{2} \cos \phi - \gamma \rho \sin \phi, \quad (2.10a)$$

$$y_c = \frac{d}{2} \sin \phi + \rho \cos \phi, \quad (2.10b)$$

with the distance ρ defined in Eq. (2.6). From Eqs. (2.10), standard algebraic manipulations allow us to express the angular coordinate ψ of the adhesion sites in the frame of the ellipse (Figure 2.4a), namely:

$$\tan \psi_0 = \frac{d \sin \phi + 2\rho \cos \phi}{d \cos \phi - 2\gamma\rho \sin \phi}, \quad (2.11a)$$

$$\tan \psi_1 = \frac{d \sin \phi - 2\rho \cos \phi}{d \cos \phi + 2\gamma\rho \sin \phi}. \quad (2.11b)$$

Illustrations of the possible configurations described by Eqs. (2.11) are shown in Figures 2.4b-e. When ρ becomes imaginary, the two adhesion sites are as far apart as possible along the ellipse. This sets the position of the extremum of the curves displayed in Figure 2.4b.

2.6.2 Material parameters for different cell types

Section 2.3 gives the material parameters γ , λ_{\min} , σ and α for a set of 285 cells. These cells, in fact, come from a pool of two different cell types. The GE11 cells used exhibit an epithelioid morphology whereas the GD25 cells exhibit a fibroblastoid morphology. Both cell types are deficient of the fibronectin receptor integrin $\beta 1$. In both cell types then either $\alpha 5\beta 1$ was reexpressed, or $\alpha v\beta 3$ was expressed. These cells are designated GE $\beta 1$, GE $\beta 3$, GD $\beta 1$ and GD $\beta 3$. The differing cell and integrin types result in a different cell-substrate coupling leading to different material parameters for each cell and integrin expression type. It is outside the scope of this chapter to examine these differences in detail, therefore initially only the average of each parameter over all 285 cells is given. For completeness, we give the same parameters per cell type in Table 2.2. As can be expected [172], cells expressing $\beta 1$ exert higher traction forces than cells expressing $\beta 3$, which is reflected in a lower λ_{\min} for the latter.

Table 2.2. Survey of the average material parameters per cell type in a sample of 285 fibroblastoid and epithelioid cells. Shown are the mean and standard deviation. Whereas γ does not vary significantly, there is some variance observed in especially λ_{\min} , which appears larger for cells expressing β -integrin.

Cell type	number of cells	γ	λ_{\min} (nN)	σ (nN/ μm)	α (nN/ μm)
GE $\beta 1$	59	0.32 ± 0.14	9.8 ± 6.9	1.4 ± 1.0	2.6 ± 2.2
GE $\beta 3$	112	0.31 ± 0.19	5.5 ± 3.4	0.62 ± 0.41	1.3 ± 1.1
GD $\beta 1$	56	0.38 ± 0.26	10.6 ± 9.4	0.92 ± 0.78	1.5 ± 1.7
GD $\beta 3$	58	0.34 ± 0.25	7.9 ± 6.0	1.0 ± 0.8	2.0 ± 2.2
All	285	0.33 ± 0.20	7.6 ± 5.6	0.87 ± 0.70	1.7 ± 1.7

2.6.3 Supporting figures

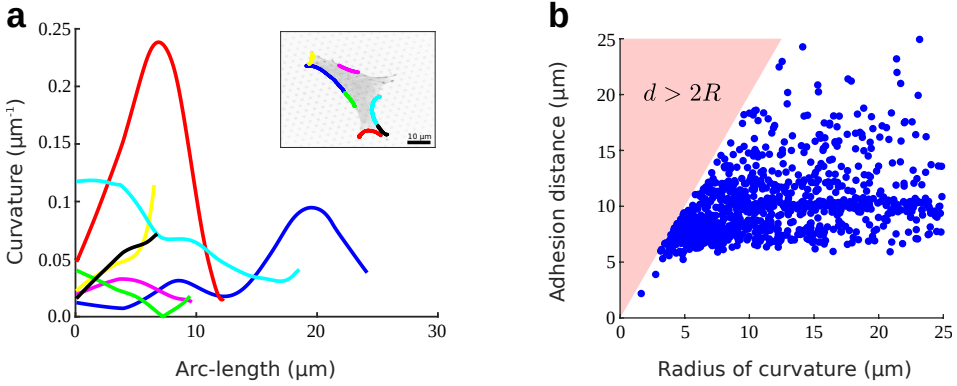


Figure 2.5. (a) Curvature versus arc-length for a specific cell (inset). The blue, red, cyan, yellow and black arcs are evidently non-circular as indicated by the smooth curvature variation. Because any smooth plane curve can be locally approximated by a circle of radius $R = 1/\kappa$, longer arcs are more likely to exhibit appreciable curvature variations. The large curvature variation of the yellow arc is instead caused by the fact that the arc is roughly perpendicular to the stress fibers, hence it experiences the largest anisotropy in the force distribution. (b) Average radius of curvature of a cellular arc versus the distance between the end-points of the arc (i.e., adhesion sites). The radius of curvature is obtained by fitting cellular arcs with circles (see Figures 2.1 and 2.7). The data points correspond to a sample of 285 cells and do not allow conclusive statements about a possible correlation between the arc's length and curvature.

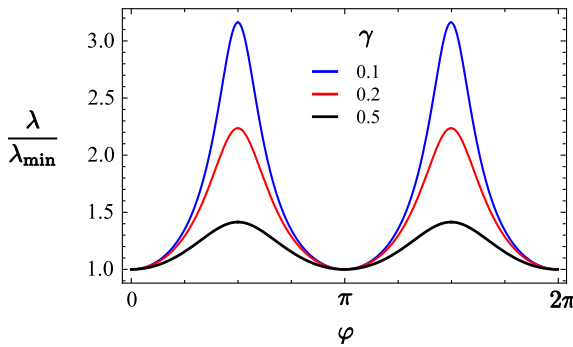


Figure 2.6. Normalized cortical tension λ/λ_{\min} , calculated as expressed by Eq. (2.4), versus the turning angle φ (see Figure 2.2) for $\theta_{\text{SF}} = \pi/2$ and various γ values. Upon increasing the anisotropy (decreasing γ), the cortical tension becomes progressively less uniform across the arc. The isotropic limit is recovered when $\gamma = 1$ and $\lambda = \lambda_{\min}$ along the entire cellular arc. Maximal tension is attained when $\varphi = \pi/2$ and the tangent vector \mathbf{T} is parallel to the stress fibers.

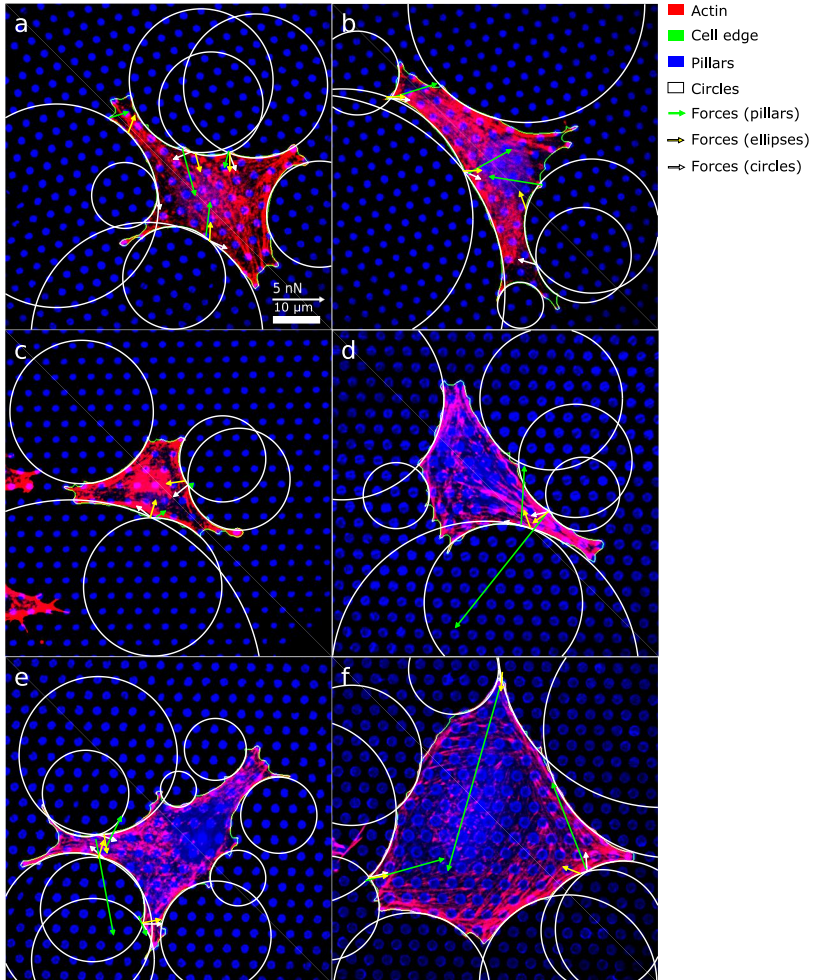


Figure 2.7. Six examples of cells with circles fitted to the cell edges. The actin, cell edge and micropillar tops are in the red, green and blue channels respectively. Circles (white) are fitted to the edge of the cells. The arrows correspond to the measured forces (green) and predicted directions (but not magnitudes) of the forces in the presence of isotropic ($\alpha = 0$, white arrow) and anisotropic ($\alpha \neq 0$, yellow arrow) contractile stresses. The length of the green arrows indicates the magnitude of the force. Green arrows originate from the center of the micropillar, while yellow and white arrows originate from the intersections of ellipses and circles respectively, therefore, arrows do not necessarily originate from the same point. Yellow and white arrows are only plotted for adhesion sites under an intersection of ellipses or circles respectively. Panels (a) to (c) show epithelioid cells and (d) to (f) show fibroblastoid cells.

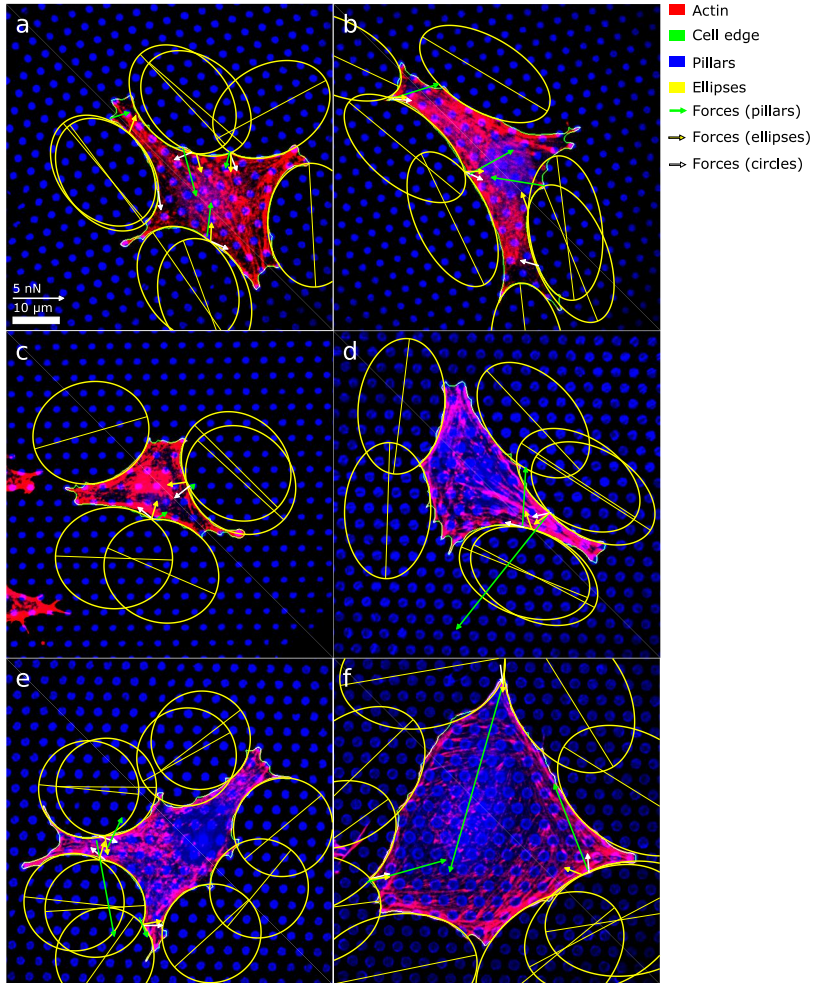


Figure 2.8. Six examples of cells (same as in Figure 2.7) with ellipses fitted to the cell edges. The actin, cell edge and micropillar tops are in the red, green and blue channels respectively. Ellipses (yellow, including the major axis) are fitted to the edge of the cells. The arrows correspond to the measured forces (green) and predicted directions (but not magnitudes) of the forces in the presence of isotropic ($\alpha = 0$, white arrow) and anisotropic ($\alpha \neq 0$, yellow arrow) contractile stresses. The length of the green arrows indicates the magnitude of the force. Green arrows originate from the center of the micropillar, while yellow and white arrows originate from the intersections of ellipses and circles respectively, therefore, arrows do not necessarily originate from the same point. Yellow and white arrows are only plotted for adhesion sites under an intersection of ellipses or circles respectively. Panels (a) to (c) show epithelioid cells and (d) to (f) show fibroblastoid cells. Fit values for the ellipses in panels (a) to (f) respectively: γ : 0.52; 0.25; 0.75; 0.40; 0.95; 0.46, λ_{\min}/σ (μm): 13.4; 15.7; 12.6; 14.7; 10.8; 18.0.

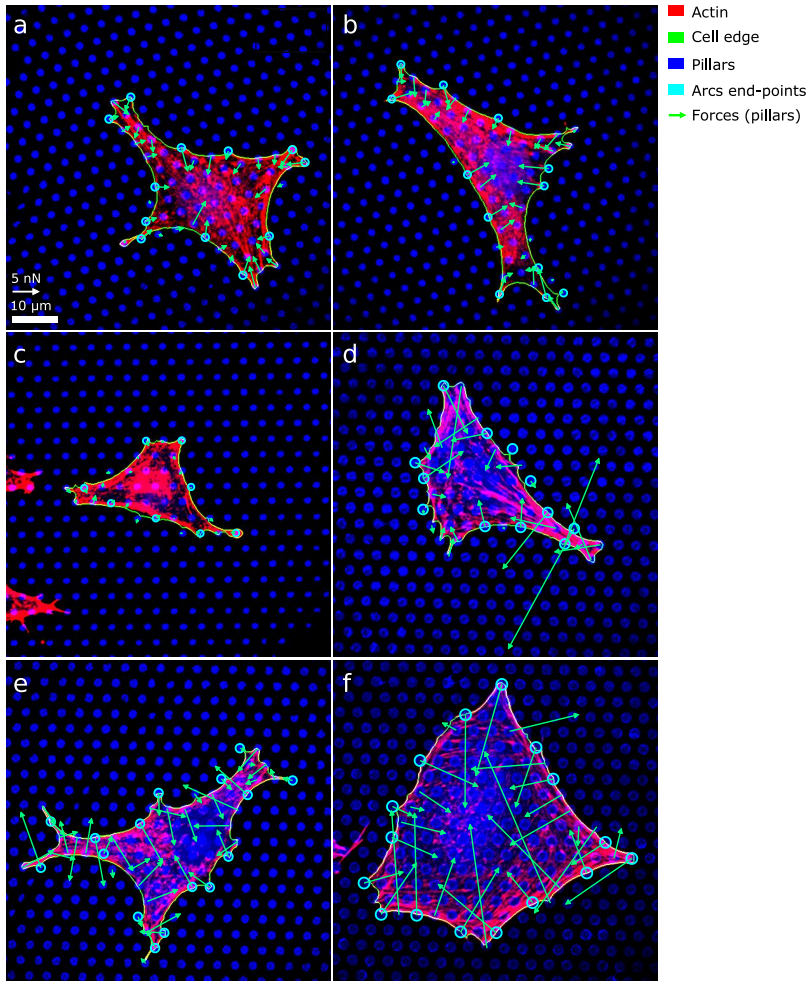


Figure 2.9. Six examples of cells (same as in Figures 2.7 and 2.8) with all the traction forces measured along the contour explicitly indicated. The actin, cell edge and micropillar tops are in the red, green and blue channels respectively. The length of the green arrows indicates the magnitude of the force and the pillars used for the geometrical fits, illustrated in Figures 2.7 and 2.8, are highlighted. Panels (a) to (c) show epithelioid cells and (d) to (f) show fibroblastoid cells.

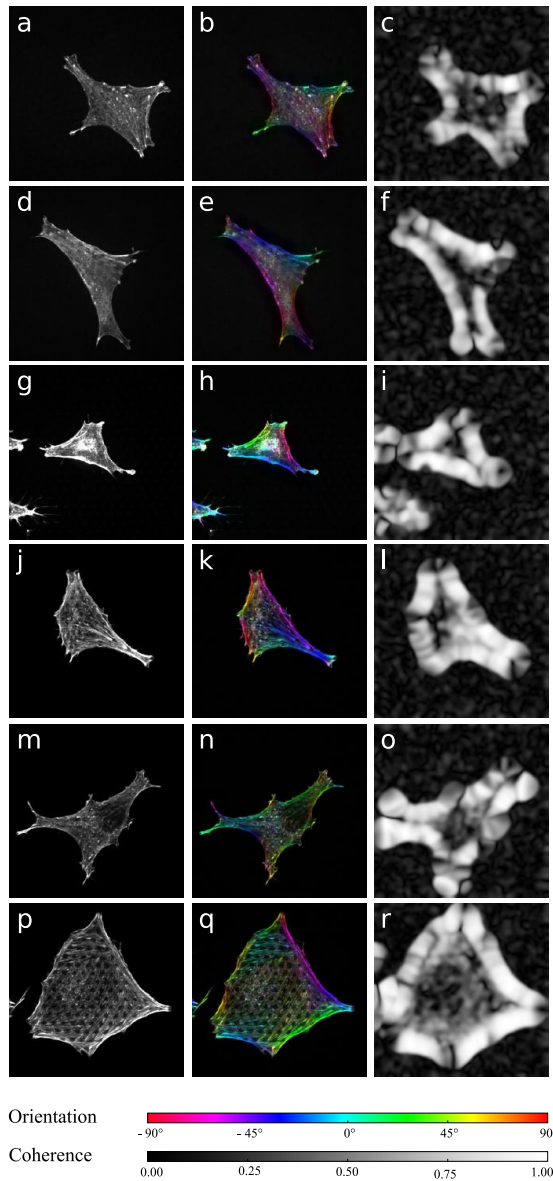


Figure 2.10. Orientational analysis of the stress fibers. On the left column, optical micrographs of the six example cells displayed in Figures 2.7, 2.8 and 2.9. On the center column, color survey of the stress fibers orientation. On the right column, density plot of the orientational coherence of the stress fibers, computed via OrientationJ [177]. Along the cell periphery, stress fibers are highly aligned and the calculated coherence is close to one (see Section 2.5.7).